5-16-2005

Hybrid Multivariable Controller Architecture

Mark A. Hopkins
Rochester Institute of Technology

David Smith
ITT Industries, Inc.

Phillip Vallone
ITT Industries, Inc.

Richard Sandor
ITT Industries, Inc.

Recommended Citation

Mark A. Hopkins, David A. Smith, Phillip Vallone, Richard Sandor, "Hybrid multivariable controller architecture", Proc. SPIE 5760, Smart Structures and Materials 2005: Damping and Isolation, (16 May 2005); doi: 10.1117/12.600191; https://doi.org/10.1117/12.600191

Hybrid multivariable controller architecture

Mark A.Hopkins[*a], David A.Smith[b], Phillip Vallone[b], Richard Sandor[b]
[a]Electrical Engineering Dept., Rochester Institute of Technology, Rochester, NY USA 14623
[b]ITT Industries, Space Systems Division, 2696 Manitou Rd., Rochester NY USA 14653

ABSTRACT

We present a multivariable controller architecture that is a hybrid combination of a classically designed controller and an observer-based controller. The design process starts with a classical multivariable feedback controller, designed by any convenient method, such as sequential SISO loop closing. After designing the classical controller, an observer-based modern controller is designed to be stable in parallel combination with the classical controller. The hybrid configuration is realized by introducing an additional feedback path between the two feedback controllers, to subtract the effects of the classical controller from the observer-state estimate. All of the controller gains are re-tuned to improve a variety of performance measures. The additional feedback path does not increase the number of states in the controller but allows significantly higher gains to be used in the observer-based controller, resulting in better isolation from input disturbances. A six-input, nine-output lightweight space structure (LSS) provides a working example. The classical controller was implemented as six 40^{th}-order SISO feedback controllers, at a sample rate of 20 kHz, closed in parallel around the six main mount struts, achieving very good isolation across the struts. A 240^{th}-order observer-based modern controller, also at a 20 kHz sample rate, was designed to work with the classical closed loops and has been implemented in the hybrid configuration described. This non-square modern controller uses feedback signals from three non-collocated sensors, in addition to the six used by the classical SISO controllers, and improves isolation by about 5 dB in the most critical regions of the controller bandwidth.

Keywords: MIMO multivariable hybrid control controller architecture flexible lightweight space structure

1. INTRODUCTION

In some multivariable control applications, judicious use of classical controller-design methods can result in very good closed-loop performance, particularly when judged in terms of input disturbance isolation. In some cases, it may even be difficult to design a modern controller that outperforms the isolation of a good classical design. For example, the linear quadratic regulator/loop transfer recovery (LQR/LTR) design method tends to improve pole damping rather than isolation, because the penalty function is typically based in the time domain.

Moreover, LQR/LTR methods can also result in pole-zero cancellations (from the input/output perspective) rather than additional damping[1]. That may be unacceptable if closed-loop poles become significantly lighter damped as they move nearer to their canceling zeros, because the closed-loop system will be more susceptible to unmodeled input disturbances, as well as more sensitive to output disturbances.

While it is possible to recast LQR in the frequency domain ñ and, of course, there are several other modern controller design approaches ñ it is nevertheless generally true that using classical methods is easier, and often more intuitive, than using modern methods. Together with the fact that classical methods can result in very good performance, these are strong arguments in favor of using classical controllers in multivariable systems, where possible.

Two of the weaknesses of classical controller-design methods are (1) the difficulty of applying them to non-square systems, and (2) the difficulty of incorporating feedback from highly non-collocated sensors. On the other hand, these are somewhat routine circumstances for modern control-design methods, leading us to consider combining the two types of controller, so as to benefit from the strengths of both.

This paper is organized as follows.
Section 2 discusses the plant to be controlled.
Section 3 discusses the plant and controller models.

[*] mark.hopkins@rit.edu; phone 1 585 475 6640; fax 1 585 475 5845

Smart Structures and Materials 2005: Damping and Isolation, edited by Kon-Well Wang,
Proceedings of SPIE Vol. 5760 (SPIE, Bellingham, WA, 2005)
0277-786X/05/$15 · doi: 10.1117/12.600191

Section 4 presents the control problem we investigated.
Section 5 presents and discusses closed-loop results for a classically designed controller.
Section 6 develops a hybrid combination of classical and observer-based controllers.
Section 7 presents a comparison of the hybrid controller results to the classical-only controller results.
Section 8 is a brief conclusion.

2. The plant

The system under consideration is a lightweight space structure (LSS). Without going into detail, suffice it to say that the LSS consists of an outer structure isolated from the ìgroundî by six active main-mount struts, and an inner structure supported aboard that outer structure by six passive struts. The entire assembly has been carefully designed and implemented to be as linear as possible, and to have a first resonant mode at about 22 Hz.

The active struts are equipped with piezoceramic actuators in the axial direction, and piezoceramic load-cells (sensors) are inserted between the strut ends and the outer structure they support. These six struts, whose actuator/sensor pairs behave as if they were collocated for modes up to about 1 kHz, are the basis for the classically designed controller.

On the inner structure, three z-axis accelerometers are installed in well-separated locations that were identified as regions where significant modal activity is highly observable. Thus, these accelerometers provide good observability of the modes of the inner structure, but they are severely non-collocated relative to the strut actuators.

3. Plant and controller descriptions

The plant is described in two ways. First, there is a set of nine-output, six-input complex frequency-response data, spanning 0.2 Hz to 10 kHz at 20,000 points, approximately logarithmically spaced in frequency. These data were obtained by way of five experiments, each designed to capture the frequency response over a relatively narrow range, whose results were stitched together to cover a significantly broad spectrum ñ nearly five orders of magnitude.

Second, there are several high-order (>400 poles) discrete-time state-space models, reasonably accurate from 0.5 Hz to 400 Hz, with some accommodation for the high-frequency dynamics. These models have a sample frequency of 20 kHz, the same frequency at which the controllers are intended to run. The models were obtained from various system identification techniques (*e.g.*, FORSE[2]), as well as from a finite-element model of the LSS.

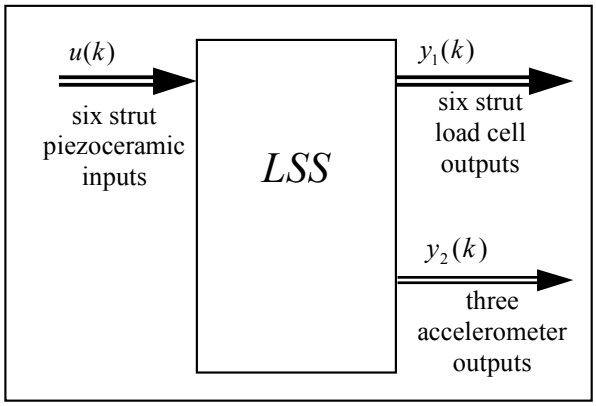

Figure 1. LSS input vector and output vectors.

In order to make it practical to run the controller in real time at 20 kHz, the observer model was reduced from a single six-input nine-output model to a set of three two-input three-output models, each with 80 poles. This step was justified by the degree to which the system exhibits three-way symmetry; and the reasonable degree of two-by-two block diagonal dominance exhibited under classical (six-input six-output) control. Each of the three observer-based controllers (80^{th}-order) is augmented in a hybrid configuration, as discussed below, by two classical 40^{th}-order SISO control loops, making each of the three controllers 160^{th}-order.

The full 480^{th}-order controller, then, is actually a set of three 160^{th}-order three-input two-output controllers. However, the tuning, the analysis, and the implementation of these controllers were always carried out in the context of the full six-input nine-output system. In effect, the nine-by-six controller is ìblock diagonalî, where each block is three-by-two.

In this paper, there are mainly two types of frequency-domain data plots. One type is the characteristic loci plot, which is used to illustrate stability margins. The six characteristic loci of the compensated open-loop system are plotted in the style of a Nichols chart, because we believe that is easier to read than a Nyquist plot.

The other type is the Frobenius norm plot. For a six-input, nine-output system, there are 54 input/output paths, and a 9x6 complex array of frequency response data at each frequency point. There are far too many to consider individual frequency response plots. In our judgment, a plot of the Frobenius norm of the frequency response matrix, versus fre-

quency, is an excellent summary of the salient features of the frequency response, particularly in conjunction with the characteristic loci.

4. Example control problem

The control objective is to provide as much input disturbance isolation as possible, over the 0 Hz to 100 Hz range, for the system being supported by the six active struts. For the purpose of analysis, it was experimentally determined that input *disturbance* isolation is essentially proportional to input isolation in this range, a characteristic that is largely attributable to the nearly ideal axial force strut support achieved in the design and fabrication of the LSS. That allows the controller design goal to be evaluated in terms of the input/output frequency response.

The LSS has several significant low-frequency modes that are strongly controllable from the strut inputs but nearly unobservable from the strut outputs, while at the same time being strongly observable from the highly non-collocated accelerometers. These modes fall in the region of 55 Hz to 75 Hz, well within the control bandwidth. Earlier experiments had verified that classical control loops around the six struts could not provide the desired level of isolation of these modes (see Figure 4, and more discussion below), because their activity is nearly unobservable at the load cell outputs.

While it is possible to mount proof mass actuators collocated with the accelerometers and then use classical control to control the 55-75 Hz modes, we were interested to know if good input isolation of these modes could be achieved without any additional actuation, using modern control methods. Thus, the plant to be controlled is defined as having six inputs and nine outputs, as shown in Figure 1.

Frobenius norms of the plant open-loop frequency responses are plotted in Figure 2, over the range from 0.2 Hz to 10 kHz. Three curves are shown, in order to illustrate the control problem. The highest curve (solid gray line) is the norm of the entire 9x6 frequency response matrix, versus frequency. The other two curves are the frequency response norms of the 6x6 subsystem comprising the strutsí inputs and outputs (dashed line), and the 3x6 subsystem comprising the six

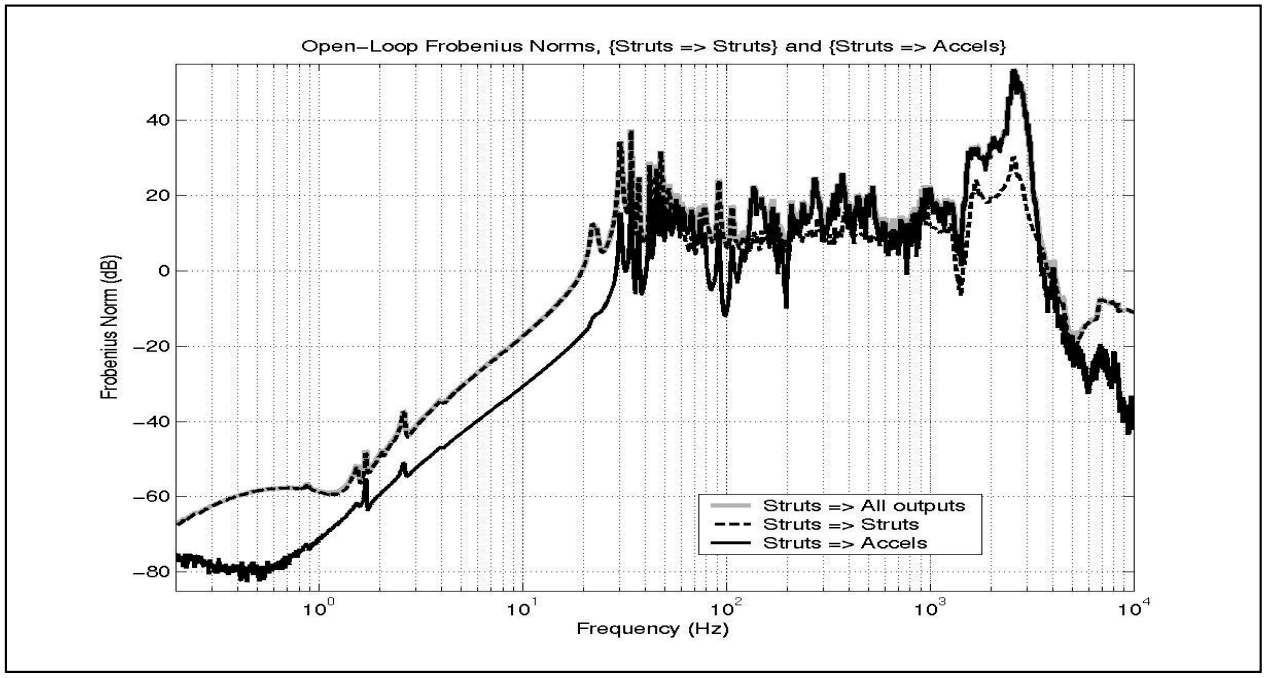

Figure 2. Frobenius norms of open-loop frequency response of the full 9x6 system, and the two subsystems (6x6 and 3x6)

strut inputs to the three accelerometer outputs (solid black line).

In Figure 2, the greater of the two subsystem norms is typically very close to the full 9x6 system norm, which indeed is the subsystemsí upper bound, so it is difficult to distinguish the gray line. Generally, modes below 100 Hz are more

observable from the strut outputs, while those above 100 Hz are more observable from the accelerometers. However, there are notable exceptions, but they are difficult to see in Figure 2.

Figure 3 presents the same data as in Figure 2, but focuses on the frequency range from 20 Hz to 100 Hz. In Figure 3, it can be seen that the modes between 55 Hz and 75 Hz are significantly more observable from the accelerometer outputs than they are from the strut load cells. The observability grammians of the models, which are quite accurate in this range, verify this characteristic. It is in this region where the classical controller does not provide as much isolation as we would like to have. The inability of the classical controller to provide the desired isolation between 55 Hz and 75 Hz, and especially at 68 Hz, is the result of insufficient observability of those modes from the strut load cells.

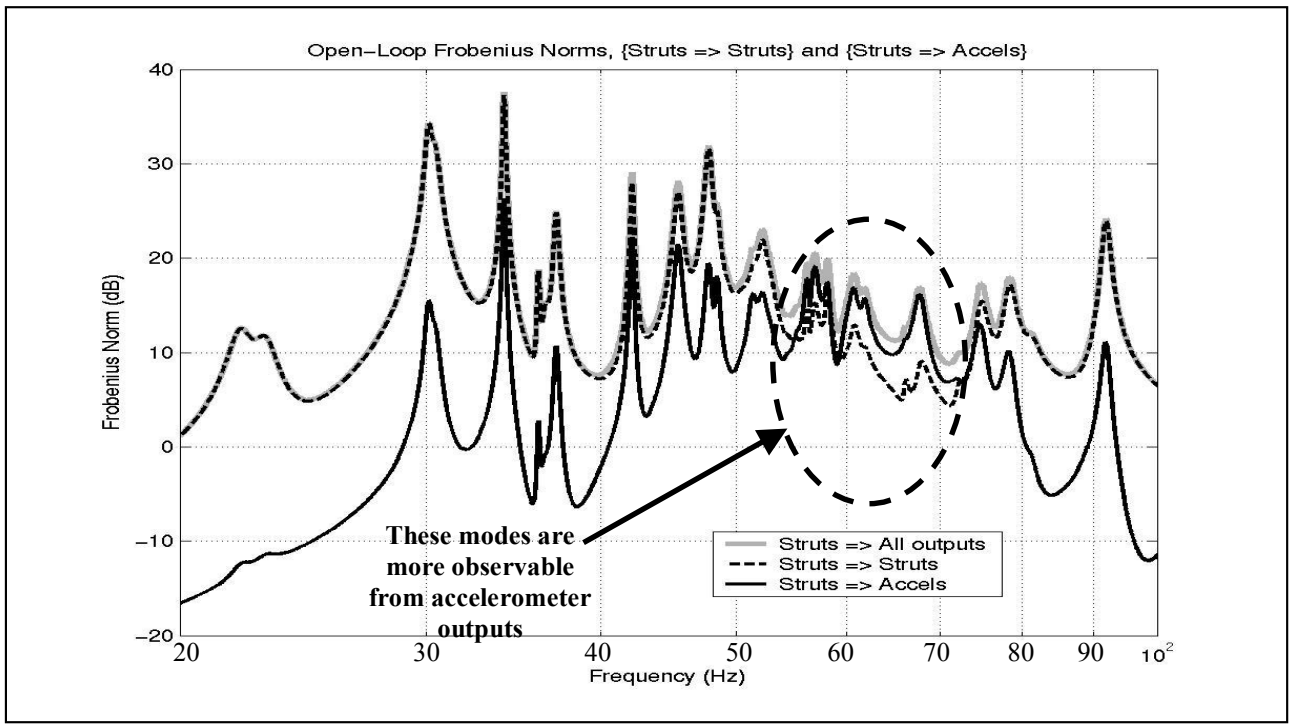

Figure 3. Frobenius norms of the open-loop frequency response (as in Figure 2), close-up of 20 Hz to 100 Hz region.

5. Classical controller results

Standard frequency-response techniques were used to design a classical SISO controller that would be stable when fitted to all six struts simultaneously. The control objective is to provide maximum input isolation up to 100 Hz, with a controller bandwidth of about 300 Hz. The classical controller provides excellent input isolation, with respect to the strut outputs, but the picture changes dramatically when viewed from the accelerometer outputs, particularly in the frequency range from 55 Hz to 75 Hz.

Figure 4 builds upon Figure 3, covering 0 Hz to 100 Hz, but it also includes the closed-loop response under classical control (six SISO loops). Again, the response is partitioned by strut outputs and accelerometer outputs. Obviously, classical control achieves quite significant input isolation, particularly when viewed from the strut outputs alone. However, when the accelerometer outputs are included in the analysis, it becomes clear that there is much less isolation in the 50 Hz to 70 Hz region than the strut outputs, alone, would indicate. More important, it provides less isolation than is required in that region.

Of greatest concern is the region from 65 Hz to 72 Hz, where the norm at the accelerometer outputs is as much as 10 dB higher than the norm at the strut outputs. Everywhere else, closed-loop isolation is close to, or even less than, ñ20 dB.

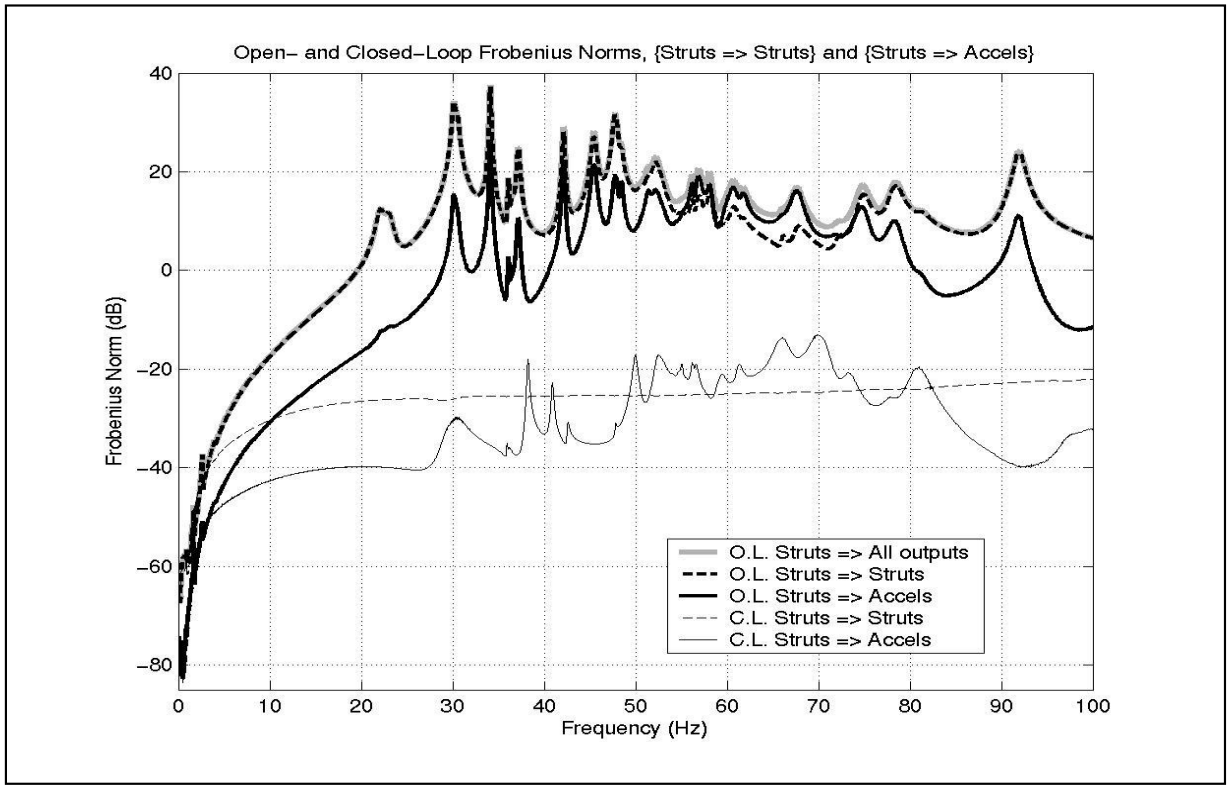

Figure 4. Frobenius norms of open-loop and closed-loop frequency response, from 0 Hz to 100 Hz. Closed-loop response is with classical control only.

Now, as illustrated by Figures 3 and 4, modes in the 55 Hz to 75 Hz region are more observable from the three accelerometer outputs than they are from the six strut outputs. This leads naturally to the idea of including the accelerometer outputs as controller inputs. That gives a non-square controller (nine feedback inputs, six control outputs), three of which are highly non-collocated with respect to the strut inputs.

6. Hybrid combination of classical and observer-based controllers

When combining two feedback controllers, one of the first questions to ask is whether or not the loops are strictly in parallel. In a strictly parallel combination, neither feedback path is making any accommodation for the control actions of the other path. That is, both controllers are trying to correct for the same output errors, effectively increasing the feedback gain.

Without modifying the essential controller structure, the only simple way to allow a classical controller to accommodate another, parallel controller, is to reduce its overall gain. There is somewhat more flexibility in allowing an observer-based controller to accommodate a parallel path. However, the resulting configuration might not be strictly parallel.

One possible configuration is to make the observer aware of the control inputs being applied to the plant by the classical feedback path. However, those classical control inputs are not at all like the standard reference inputs, which would normally be applied to the observer through its input ($\hat{B}$) matrix. Nor can they be considered the same as perturbations, since they are not random, and are highly correlated with the output. Thus, it doesnít seem correct to apply the classical controller outputs to the observer in the usual way.

Another possible configuration is to estimate what effect the classical controllerís signal is having on the internal state of the plant, and prevent the observer-based controller from trying to correct for that effect. Stated in other words, try to subtract off that part of the observer-based controllerís feedback that is attempting to correct for excitations that are due to the classical controllerís activities.

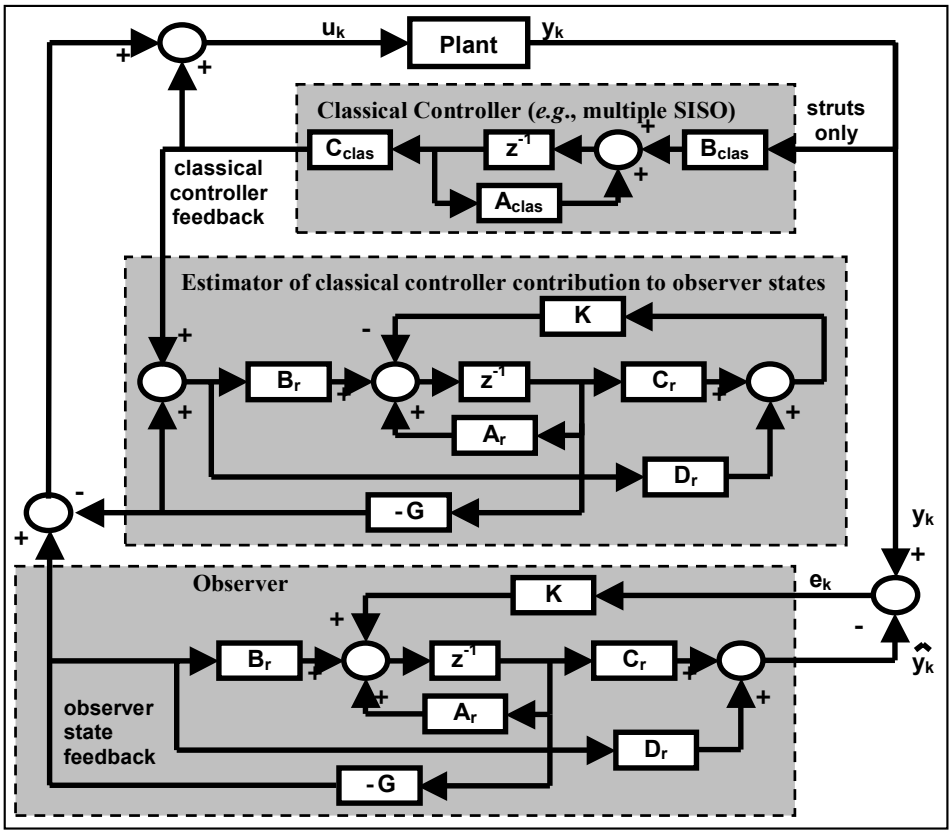

Figure 5. Closed-loop configuration with separate observer for classical controller effects.

Figure 5 shows the latter interpretation of this configuration. Two identical observer-based controllers are used, one being driven by the plant output, and the other being driven by the classical control signal. The plant-output driven observer is intended to estimate the state of the plant, while the classical control-input driven observer estimates only that part of the state attributable to the classical control signal. When these observersí feedback signals are combined, the idea is to subtract out that portion of the control signal that is attempting to correct for the classical controller input.

Notation in Figure 5 corresponds as follows. The classical controller is implemented in state-space form $\{A_{clas},B_{clas},C_{clas},D_{clas}\}$, in which $D_{clas} = \mathbf{0}$. The observer-based controller is based on reduced-order system model $\{A_r,B_r,C_r,D_r\}$, with internal observer feedback matrix K, and state-feedback gain matrix G. The high-order model (from which the observerís reduced-order model may have been obtained) will be denoted simply $\{A,B,C,D\}$.

The observer-based controller blocks of Figure 5 can be manipulated to the form shown in Figure 6, which makes their congruency more apparent. Because they are congruent, the two controllers may be combined, as in Figure 7. Finally, both the classical controller and the observer-based controller can be folded into a single controller, as in Figure 8.

Assuming high-order plant model $\{A,B,C,D\}$, the closed-loop model shown in Eq.1 can be extracted from Figure 8. Let x_k denote the plant states, $\hat{x}_k$ the observer states, and $\bar{x}_k$ the states of the classically designed controller. The eigenvalues of the matrix in Eq.1 are estimates of the *closed-loop poles*.

$$\begin{bmatrix} x_{k+1} \\ \hat{x}_{k+1} \\ \bar{x}_{k+1} \end{bmatrix} = \begin{bmatrix} A & -BG & BC_{clas} \\ KC & A_r - KC_r - [B_r + K(D - D_r)]G & -(B_r - KD_r)C_{clas} + KDC_{clas} \\ B_{clas}C & -B_{clas}DG & A_{clas} + B_{clas}DC_{clas} \end{bmatrix} \begin{bmatrix} x_k \\ \hat{x}_k \\ \bar{x}_k \end{bmatrix} \qquad \textbf{Eq.1}$$

For the purpose of estimating *transmission zeros*, the compensated open-loop model is found by opening the feedback path from compensator to plant input, while preserving the path from plant output to compensator. This includes separating out state-feedback paths that are attributable to loop closure, as shown in Eq.2. Note that the resulting system is square, with an equal number of inputs and outputs (*i.e.,* the strut inputs, and the control signals that will go to those struts in closed-loop configuration).

$$\begin{bmatrix} x_{k+1} \\ \hat{x}_{k+1} \\ \bar{x}_{k+1} \end{bmatrix} = \begin{bmatrix} A & \mathbf{0} & \mathbf{0} \\ KC & A_r - KC_r & -2[B_r - K(D - D_r)]C_{clas} \\ B_{clas}C & \mathbf{0} & A_{clas} \end{bmatrix} \begin{bmatrix} x_k \\ \hat{x}_k \\ \bar{x}_k \end{bmatrix} + \begin{bmatrix} B \\ B_r + K(D - D_r) \\ B_{clas}D \end{bmatrix} \begin{bmatrix} \mathbf{0} & -G & C_{clas} \end{bmatrix} \begin{bmatrix} x_k \\ \hat{x}_k \\ \bar{x}_k \end{bmatrix} \quad \textbf{Eq.2}$$

Eq. 2 can be recast as an open-loop state-space model (note that its ìDî matrix is zero):

$$\begin{bmatrix} x_{k+1} \\ \hat{x}_{k+1} \\ \bar{x}_{k+1} \end{bmatrix} = \begin{bmatrix} A & \mathbf{0} & \mathbf{0} \\ KC & A_r - KC_r & -2[B_r - K(D - D_r)]C_{clas} \\ B_{clas}C & \mathbf{0} & A_{clas} \end{bmatrix} \begin{bmatrix} x_k \\ \hat{x}_k \\ \bar{x}_k \end{bmatrix} + \begin{bmatrix} B \\ B_r + K(D - D_r) \\ B_{clas}D \end{bmatrix} u_k \quad \textbf{Eq.3}$$

$$y_k = \begin{bmatrix} \mathbf{0} & -G & C_{clas} \end{bmatrix} \begin{bmatrix} x_k \\ \hat{x}_k \\ \bar{x}_k \end{bmatrix}$$

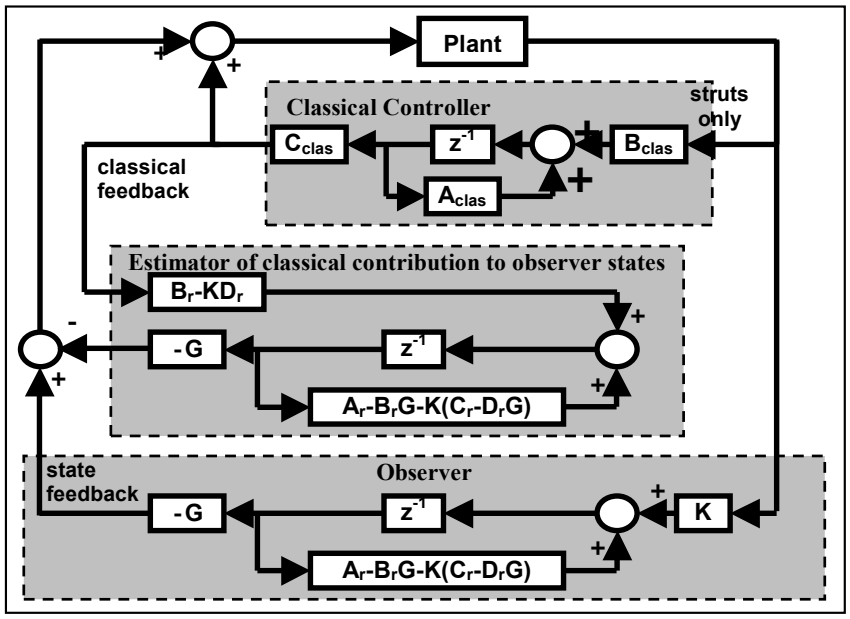

Figure 6. Closed-loop configuration of Figure 4, rearranged to emphasize congruency of the two observer-based controllers.

Note that the closed-loop system of Eq.1 can be obtained from Eq.3 by letting $u_k = y_k$.

For the purpose of computing *characteristic loci*, frequency response of the compensated open loop is calculated based on the *measured* open-loop system frequency-response (rather than the state-space modelís frequency response) in series with the frequency response of the stand-alone compensator. Using the measured frequency-response makes the characteristic loci computation model-independent, hence more accurate. For the hybrid controller, the stand-alone configuration is extracted either from Eq.1 or from Figure 8.

For instance, to extract the stand-alone configuration from Eq.1, one would subtract off the system feedthrough terms that occur in closed-loop (namely, all terms involving matrix D of the full-order model), and represent the plant contribution to controller states in terms of its output $y_k = Cx_k + Du_k$, rather than its states. The stand-alone controller configuration is given in Eq.4.

$$\begin{bmatrix} \hat{x}_{k+1} \\ \bar{x}_{k+1} \end{bmatrix} = \begin{bmatrix} A_r - KC_r - B_rG + KD_rG & -(B_r - KD_r)C_{clas} \\ \mathbf{0} & A_{clas} \end{bmatrix} \begin{bmatrix} \hat{x}_k \\ \bar{x}_k \end{bmatrix} + \begin{bmatrix} K \\ B_{clas} \end{bmatrix} y_k$$

$$u_k = \begin{bmatrix} -G & C_{clas} \end{bmatrix} \begin{bmatrix} \hat{x}_k \\ \bar{x}_k \end{bmatrix} \quad \textbf{Eq.4}$$

Note that the additional path from classical controller to observer-based controller has no effect on the open-loop poles of the controller, evident by the block diagonal structure of the system matrix in Eq.4.

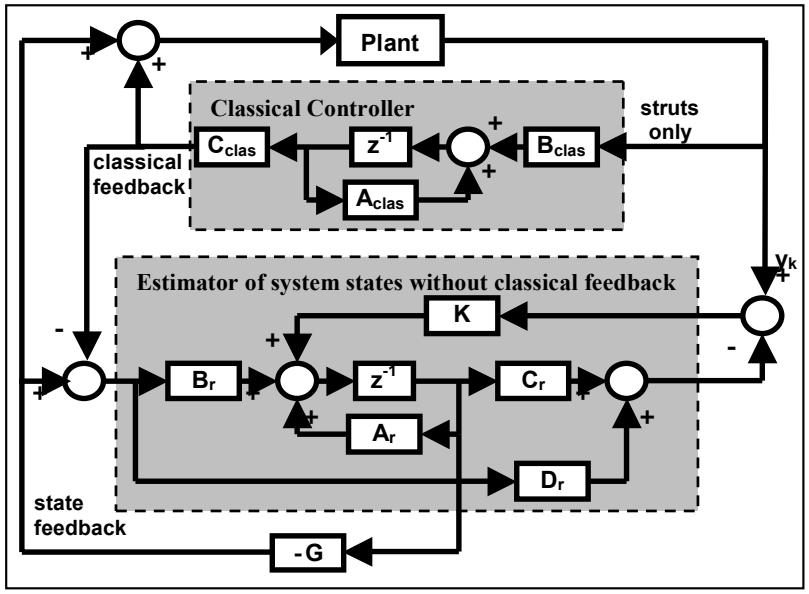

Figure 7. Closed-loop configuration with a combined observer taking into account the effects of both driving signals.

7. Hybrid controller results

Figure 9 builds upon Figures 3 and 4, covering 0 Hz to 100 Hz but also including the closed-loop response under the hybrid controller. Again, the response is partitioned by strut outputs and accelerometer outputs. Inclusion of the observer-based controller in the hybrid configuration can be seen in Figure 9 to improve the input isolation in the 55 Hz to 75 Hz region, without significantly affecting it elsewhere.

Figure 10 is a close-up of the same data presented in Figure 9, focusing on the closed-loop norms only, and only between 50 Hz and 80 Hz. Across this frequency range, the hybrid controller improves isolation, on average, by about 2 dB compared to the classical-only controller. Of particular interest is the fact that isolation is improved by as much as 5 dB in the most important part of this range, between 65 Hz and 70 Hz, and especially at 68 Hz. Figure 10 also shows that the hybrid controller improves isolation not only from the strut inputs to the accelerometer outputs, but from the strut inputs to the strut outputs, as well.

The same classical controller is used in the hybrid controller as is used in the classical-only analysis. The hybrid controller required significant tuning to achieve good stability margins, in addition to the desired increases in isolation. The stability margins are indicated by the characteristic loci plotted in Figures 11, 12, and 13.

Each of the three characteristic loci plots (Figures 11, 12, and 13) show all six of the characteristic loci of the open-loop compensated system. These are gray-scale plots, because even if they had been included as color plots, it would not be particularly informative to follow any individual loci. Rather, it is encirclements of the critical point -1, or intrusion of any loci into the neighborhood close to the critical point that require attention. In Figure 11, the lack of encirclements indicates that the hybrid controller is predicted to be absolutely stable.

Because these plots are in Nichols format (magnitude in dB versus phase in degrees), rather than Nyquist, the critical point actually shows up in more than one place, namely, every point along the 0 dB magnitude line where phase is an odd-integer multiple of 180 degrees. For example, in Figure 11, the critical point can be seen in two locations, [0 dB, $+180^o$] and [0 dB, -180^o].

In Figure 11, it is not difficult to see that very good relative stability margins are predicted for the hybrid controller in the low frequency region, where the characteristic loci stay well away from the point [0 dB, $+180^o$]. The high frequency region is less clear, because the loci seem to crowd the point [0 dB, -180^o]. For that reason, Figure 12 provides a close-up of the neighborhood around the point [0 dB, -180^o].

In the close-up of Figure 12, it is much clearer that the hybrid controller also has reasonable stability margins in the high frequency regions. What is not obvious is whether those margins are attributable to the classical part of the hybrid controller, or to the observer-based controller part. Figure 13 is included to address that question.

Figure 13 shows the characteristic loci of the classical-only controller as gray lines, superimposed on black lines that are the characteristic loci of the hybrid controller. This figure makes it clear that stability margins have been improved by the introduction of the observer-based controller, in the hybrid configuration. The gray lines approach the critical point more closely than the black lines, at frequencies between 100 Hz and 300 Hz, and are also generally closer to the -180 degree phase line, implying that there is more likely to be a gain reduction margin (*i.e.*, a conditionally stable system).

8. CONCLUSION

A hybrid combination of multivariable classical controller and observer-based controller was derived in a series of block diagram manipulations. Equations were extracted from the diagrams, showing how to compute the closed-loop poles and transmission zeros, given a system model. The system model can be the same as the observer model, or it could be a higher-order model from which the observer model was obtained by model-order reduction techniques.

Equations were also presented showing how to compute the open-loop model of the hybrid controller, itself, which can be used to compute the hybrid controllerís transfer function. The hybrid controller transfer function can be combined with empirical frequency response data of the system to obtain the compensated frequency response, from which characteristic loci can be determined, as well as a prediction of closed-loop frequency response. The characteristic loci help to predict the relative stability of the closed-loop system, and help analyze which frequency ranges are most likely to be involved in stability problems.

A significantly complex example of an application of the hybrid controller architecture was presented. This was a lightweight space structure (LSS), instrumented with six main-mount strut actuators and sensors, and with three accelerometer outputs. The struts sensors and actuators behave very much as if they are collocated out to frequencies around 1 kHz. The accelerometer outputs are extremely non-collocated relative to the strut actuators, being mounted on a subsystem that is separated from the main-mount struts by a set of six passive struts.

Thus, the example system is non-square, having six inputs and nine outputs, and it has some outputs that are extremely non-collocated relative to the inputs. Both of these are difficult characteristics for classical controller design approaches, but are reasonably straightforward for modern controller design techniques.

Results of the hybrid controller architecture were presented that show an observer-based controller can use the accelerometersí superior observability of certain problem modes to significantly improve the isolation of those modes from the input, compared to the isolation achieved by the classical-only controller. For this structure, input isolation is known to be essentially proportional to isolation from disturbances originating on the other side of the main-mount struts.

It was also shown that inclusion of an observer-based controller in the hybrid configuration can improve the closed-loop relative stability, compared to the multivariable classical controller, alone, particularly in the range where the controller is rolling off.

Earlier hardware implementation and testing of several similar hybrid controller designs, on the actual LSS described above, have verified that closed-loop performance is very close to what is predicted by the characteristic loci and frequency response plots. Recent modifications of the structure prevented hardware testing of the specific controller reported here.

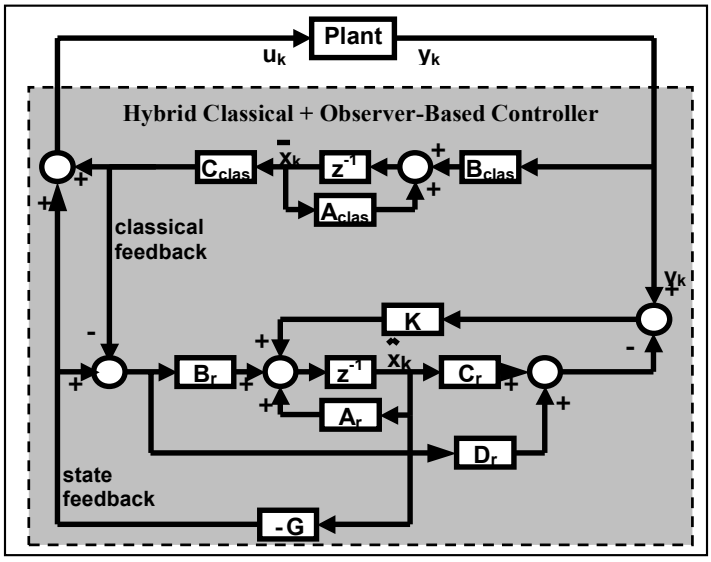

Figure 8. Closed-loop configuration, with fully combined observer-based and classical controllers.

REFERENCES

1. J. M. Maciejowski, *Multivariable Feedback Design*, Addison-Wesley Publishing Co., 1989, p.243.
2. K. Liu, R. N. Jacques, D. W. Miller, ì Frequency domain structural system identification bv observability range space extractionî , *ASME Journal of Dynamic Systems, Measurement, and Control*, **118**:2, June 1996.

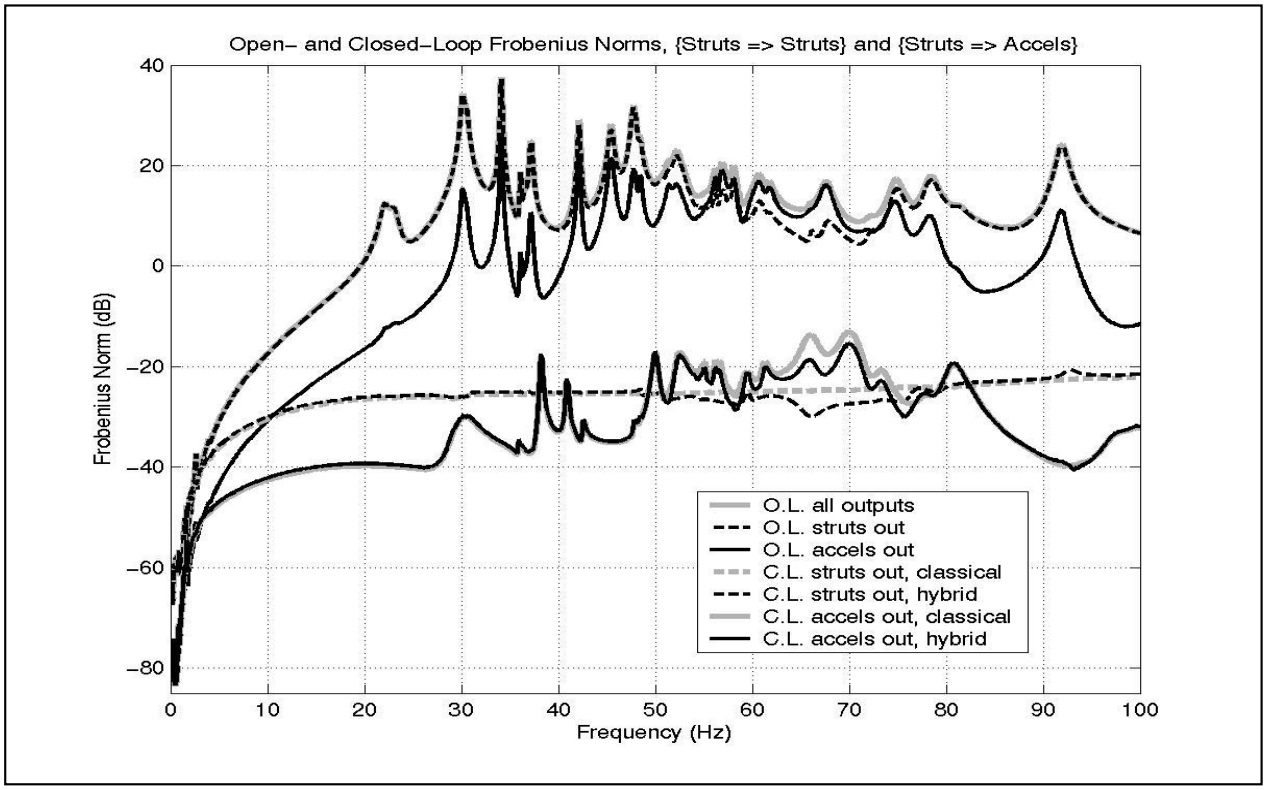

Figure 9. Open-loop and closed-loop Frobenius norms, classical and hybrid controller comparison.

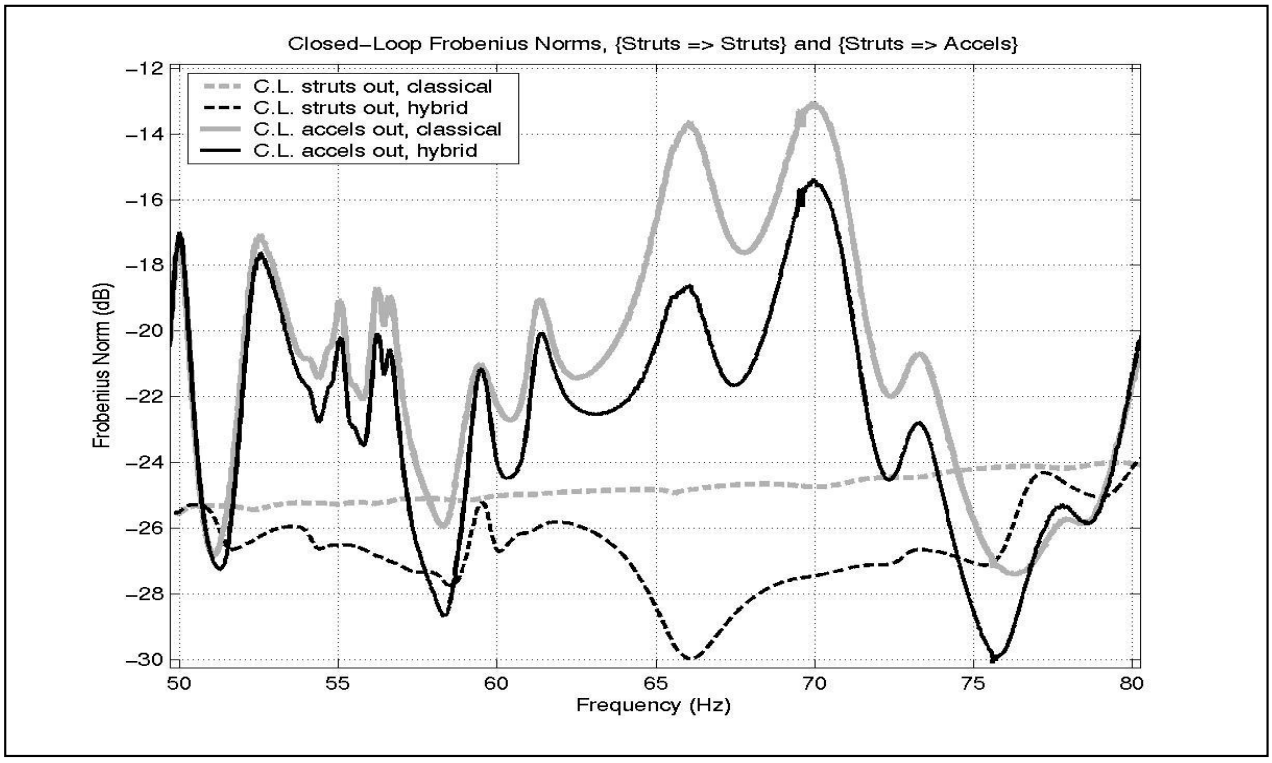

Figure 10. Closed-loop Frobenius norms, classical and hybrid controller comparison, closeup of 50 Hz to 80 Hz.

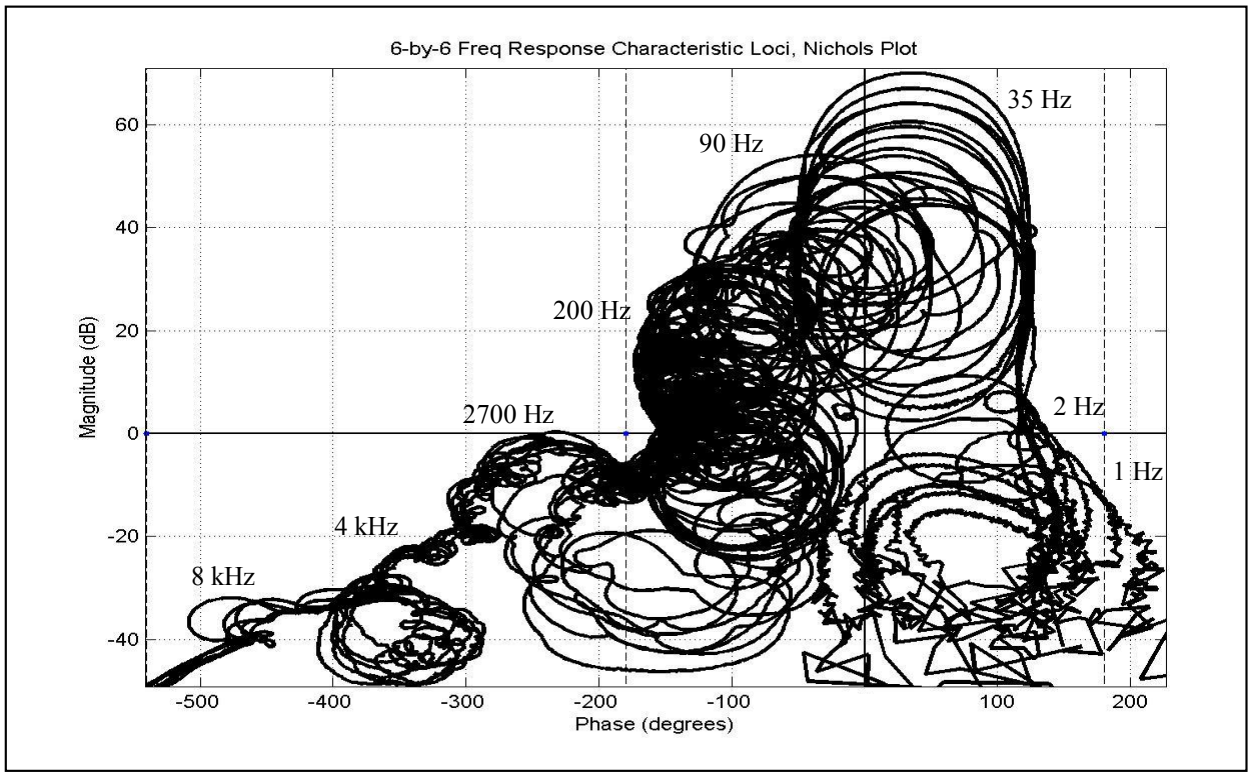

Figure 11. Six characteristic loci, from 0.5 Hz to 9 kHz. Some of the implicit frequencies are annotated.

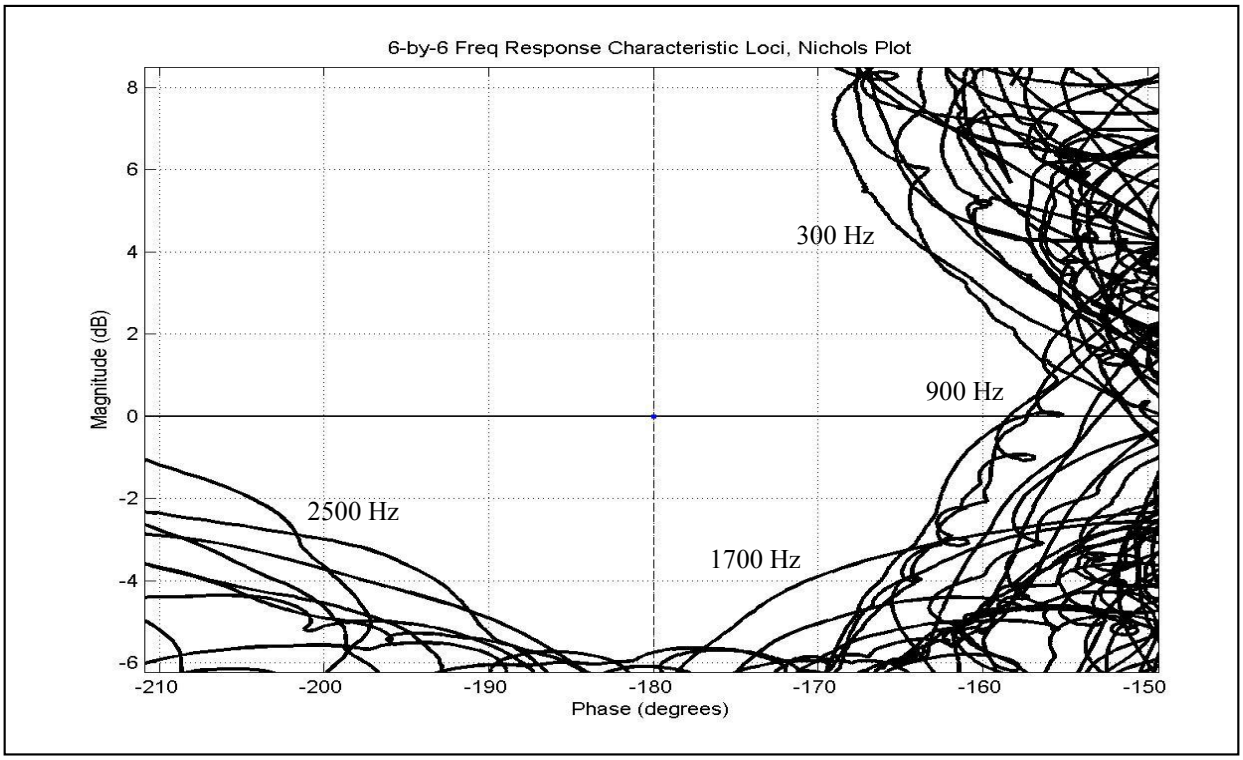

Figure 12. Six characteristic loci in the neighborhood of the critical point at [0 dB, -180^{o}].

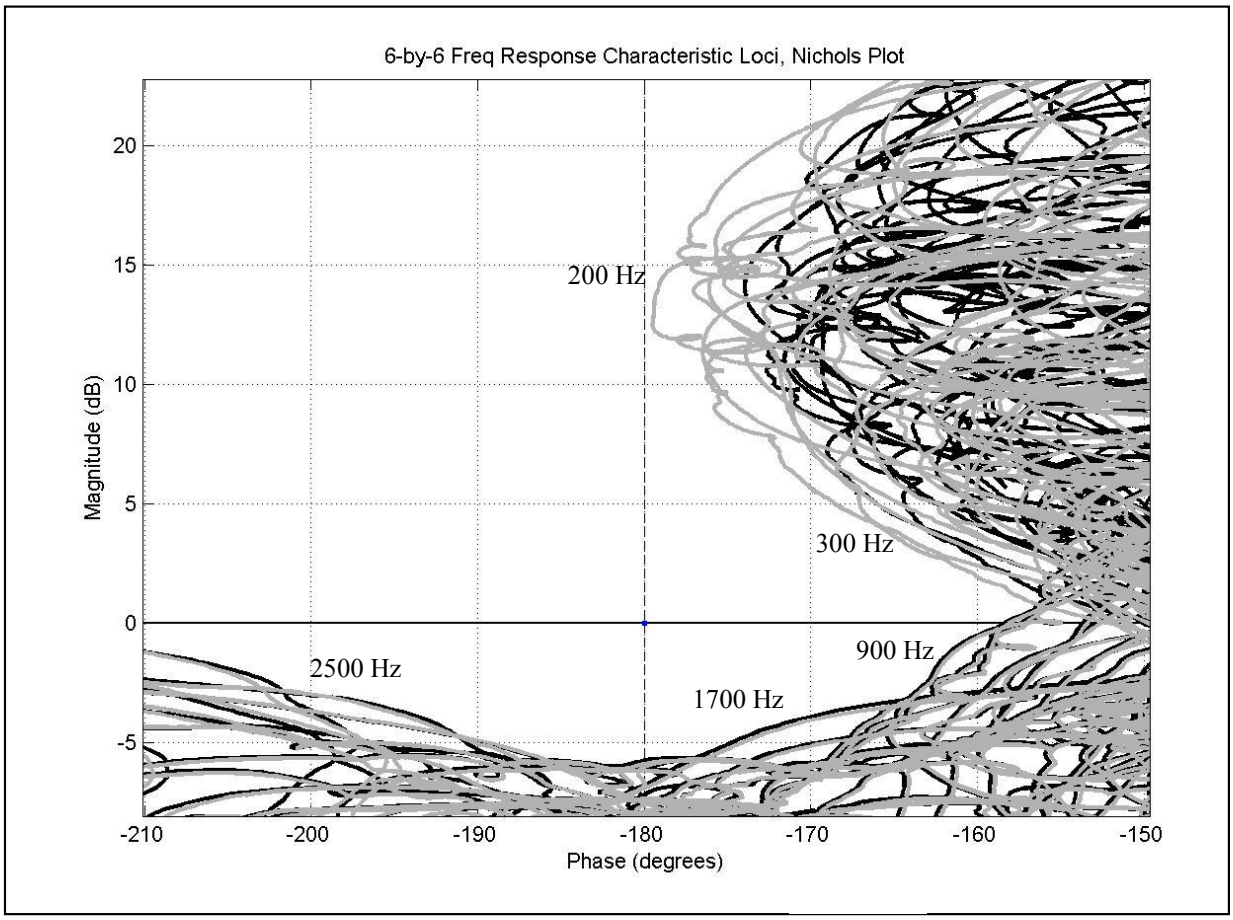

Figure 13. The six characteristic loci in high-frequency region, classical-only (grey) compared to hybrid (black) compensation. Hybrid controller improves stability margins in the rolloff region, between 100 Hz and 300 Hz.